Radio-Frequency C - V Measurements with Subattofarad Sensitivity

Malinowski, Filip K.; Han, Lin; De Jong, Damaz; Wang, Ji Yin; Prosko, Christian G.; Krogstrup, Peter; Bakkers, Erik P.A.M.; Kouwenhoven, Leo P.; Koski, Jonne V.; More Authors

DOI
10.1103/PhysRevApplied.18.024032

Publication date
2022

Document Version
Final published version

Published in
Physical Review Applied

Radio-Frequency *C-V* Measurements with Subattofarad Sensitivity

Filip K. Malinowski,[1,*] Lin Han,[1] Damaz de Jong,[1] Ji-Yin Wang,[1] Christian G. Prosko,[1] Ghada Badawy,[2] Sasa Gazibegovic,[2] Yu Liu,[3] Peter Krogstrup,[3] Erik P.A.M. Bakkers,[2] Leo P. Kouwenhoven,[1] and Jonne V. Koski[4]

[1] *QuTech and Kavli Institute of Nanoscience, Delft University of Technology, Delft 2600 GA, Netherlands*
[2] *Department of Applied Physics, Eindhoven University of Technology, Eindhoven 5600 MB, Netherlands*
[3] *Center for Quantum Devices, Niels Bohr Institute, University of Copenhagen & Microsoft Quantum Materials Lab Copenhagen, Lyngby, Denmark*
[4] *Microsoft Quantum Lab Delft, Delft University of Technology, Delft 2600 GA, Netherlands*

(Received 8 October 2021; revised 14 June 2022; accepted 16 June 2022; published 11 August 2022)

We demonstrate the use of radio-frequency (rf) resonators to measure the capacitance of nanoscale semiconducting devices in field-effect transistor configurations. The rf resonator is attached to the gate or the lead of the device. Consequently, tuning the carrier density in the conducting channel of the device affects the resonance frequency, quantitatively reflecting its capacitance. We test the measurement method on InSb and InAs nanowires at dilution-refrigerator temperatures. The measured capacitances are consistent with those inferred from the periodicity of the Coulomb blockade of quantum dots realized in the same devices. In an implementation of the resonator using an off-chip superconducting spiral inductor we find the measurement sensitivity values reaching down to 75 zF/$\sqrt{\text{Hz}}$ at 1 kHz measurement bandwidth, and noise down to 0.45 aF at 1 Hz bandwidth. We estimate the sensitivity of the method for a number of other implementations. In particular, we predict a typical sensitivity of about 40 zF/$\sqrt{\text{Hz}}$ at room temperature with a resonator composed of off-the-shelf components. Of several proposed applications, we demonstrate two: the capacitance measurement of several identical 80-nm-wide gates with a single resonator, and the field-effect mobility measurement of an individual nanowire with the gate capacitance measured *in situ.*

DOI: 10.1103/PhysRevApplied.18.024032

I. INTRODUCTION

Radio-frequency (rf) resonators are broadly used for readout of solid-state qubits, whether the quantum information is encoded as an excitation of a superconducting circuit [1], a quantum dot's charge, or an electronic spin [2]. This follows from mappings of the equivalent resistance, capacitance, or inductance of the quantum system to the transmission or reflection coefficient of the macroscopic rf resonator. Furthermore, resonance frequencies between tens of megahertz and tens of gigahertz enable the use of near-quantum-limited cryogenic amplifiers, with noise temperatures below 1 K [3,4]. Seminal work of Schoelkopf *et al.* [5] demonstrated an orders-of-magnitude improvement in electrometer sensitivity, once the low-frequency measurement of the single-electron transistor is substituted by embedding it in a rf resonator [6].

Concurrently, a number of methods have been developed to measure capacitance of field-effect transistors (FETs), Schottky junctions, and various other semiconducting devices [7–10]. A common feature of these measurement schemes is the use of relatively low excitation frequencies, up to tens of kilohertz, raising a question of whether a scheme similar to that of Ref. [5] could also improve the sensitivity of capacitance measurements. Such an approach would increase the measurement bandwidth and reduce the influence of the ubiquitous $1/f$ noise by several orders of magnitude. Instead, the measurement would become limited by much smaller Johnson-Nyquist noise, amplifier noise, and noise intrinsic to the device.

Indeed, the principle of mapping the conductance and resistance on the frequency and quality factor of a rf resonator, respectively, is widely adopted in studies of gate-defined semiconducting quantum dots [6,11–15]. In these cases, the discrete electron charge tunnels between the dots or between the dot and the lead at a well-defined gate voltage, giving rise to a relatively large effective capacitance at the charge transition. In a number of works, when the

*f.k.malinowski@tudelft.nl

tunneling is spin dependent, rf capacitance measurement was used to perform high-fidelity readout of a spin qubit [16–18] down to a few-microsecond timescale [19].

We suggest that rf capacitance measurements can be used in studies of micro- and nanoscale semiconducting devices more broadly [6]. In particular, in the absence of a quantum dot enhancing the capacitance at the charge transition, the magnitude of the signal is significantly decreased, requiring much smaller measurement bandwidth. To date, several groups reported the sensitivities in the range from 50 to 100 $zF/\sqrt{Hz}$, but these values were benchmarked by measuring the magnitude of a sideband peak under modulation of capacitance [4,20]. This method compares the magnitude of the signal against the noise background around resonance frequency, which may not straightforwardly translate to equivalent performance for long measurement times.

To explore the performance of radio-frequency capacitance measurements in long measurements, we characterize the bulk capacitance of semiconducting nanowire devices in a FET configuration. The resonance frequency is measured as a function of gate voltages, and we demonstrate that the frequency shift quantitatively matches the gate capacitance, extracted independently from the periodicity of the Coulomb blockade.

We benchmark the sensitivity of this measurement method for long measurement times, where the relevant noise spectrum is frequency dependent. We find that while the absolute noise is reduced for bandwidths below 1 kHz, the corresponding sensitivity deteriorates by about an order of magnitude from 70 $zF/\sqrt{Hz}$ at 1 kHz to 500 $zF/\sqrt{Hz}$ at 1 Hz. By measuring the noise spectra we attribute the deterioration of sensitivity to an onset of $1/f$ noise and switching of two-level systems in the vicinity of the device, illustrating the limitations of the sensitivity as a metric of the measurement precision. Nonetheless, with such performance, moderate integration times (< 1 s) are sufficient to measure capacitances of devices with a footprint below 100 nm, as well as quantum contributions to a bulk capacitance of other devices with a typical scale of about 1 μm [21,22].

In Sec. II, we introduce the principle of the capacitance measurement with a rf resonator, and discuss its variants and limitations. Section III presents a validation of the method by comparing the capacitance extracted from the resonator shift with that extracted from the periodicity of the Coulomb blockade in three devices with different gate sizes. In Sec. IV we characterize the sensitivity and the noise of the capacitance measurement, and estimate the performance of the method for several different temperatures, amplifiers, and realizations of rf resonators. Section V presents the application of the method to measure uniformity of nominally identical gates and to measure field-effect mobility of an individual device. We also discuss several other possible applications and implementations.

II. METHOD

The measurement method is based on the elementary fact that the resonance frequency of an LC circuit depends on its capacitance. Therefore, if the inductance L embedded in the circuit is known, one can infer the capacitance from a measurement of the resonance frequency. To this end, the resonance frequency is extracted from the frequency-dependent reflection or transmission through the resonator. In this section we describe how to apply this principle to measure the capacitance of mesoscopic devices. We start by describing the devices used for the validation of the method. Next we outline the experimental procedure. We conclude the section with a discussion of a number of critical factors that need to be taken into account in order for the method to yield valid results.

The nanostructures used for validation and benchmarking of the method are InSb and InAs nanowire single-electron transistors, depicted schematically in Fig. 1(a). The nanowires are grown by metalorganic vapour-phase epitaxy (InSb) [23] or molecular beam epitaxy (InAs) [24], and deposited on a highly resistive Si substrate. The devices are bottom gated in the case of InSb, and top gated in the case of InAs. The Ti/Au gates for tuning the electron density in the bulk of the nanowire are defined by electron-beam lithography and are isolated from the wire by about 15 nm of ALD AlO_x. Source and drain contacts are made of Ti/Au and deposited with a direct contact to the nanowire. In these devices, we aim to characterize the capacitance C_G between the central gate and the nanowire as a function of the applied voltage V_G. For that purpose, we wire bond the source or the central gate of each measured device to superconducting (Nb, Ti)N spiral inductor resonators [25] with inductances between 420 and 730 nH. Together with the parasitic capacitance and self-capacitance (typically 0.3–0.35 pF), these inductors form LC circuits with resonance frequencies between 300 and 500 MHz. The barrier gate voltages, $V_{L/R}$, locally tune the electrostatic potential in order to connect or isolate the bulk of the wire from the contacts, or to form tunnel barriers. The reflection from the resonators is measured using a Rhode&Schwarz ZNB 20 vector network analyzer, with a cryogenic Cosmic Microwave CITLF2 HEMT amplifier used in the first step of the amplification chain.

Figure 1(b) depicts a schematic of the circuit for the capacitance measurement with the rf resonator connected to the source of the device. Voltage V_L is set to provide a good galvanic connection [26] between the contact and the tuneable bulk of the nanowire. Voltage V_R is such that the nanowire is locally fully depleted to disconnect the drain contact that would otherwise act as a rf ground. Next, the reflection from the resonator is measured to extract the

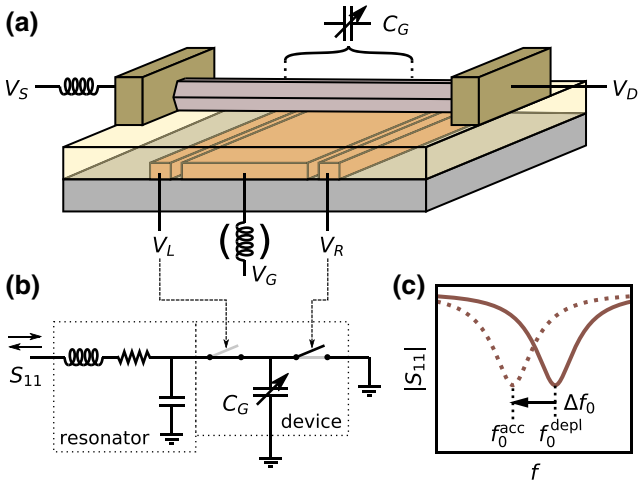

FIG. 1. (a) Schematic of a bottom-gated nanowire device in a FET configuration. A source-drain voltage $V_{SD} = V_S - V_D$ can be applied to measure the conductance of the device. Gate voltages $V_{L/G/R}$ control the electron density in the semiconductor. Here C_G symbolizes the variable capacitance between the gate and the segment of the nanowire tuned by the gate voltage V_G. Coil symbols indicate contacts that can be connected to a rf resonator to perform capacitance measurements. (b) Schematic of the circuit for the capacitance measurement with the resonator attached to the device source contact. A lossy resonator is represented as a RLC circuit. The device is represented as two switches (tuned by gate voltages $V_{L/R}$) and a variable capacitor. For a capacitance measurement, the gate voltage V_L is set to accumulate charge carriers, while V_R is set to deplete them. (c) Illustration of the resonance frequency shift, measured in reflectometry, resulting from the accumulation of electrons in the nanowire. In the measured nanometer-scale devices the frequency shifts are typically much smaller than the resonance linewidth.

resonance frequency as a function of the gate voltage V_G. Figure 1(c) schematically illustrates that in the reflection measurement the resonance frequency is reduced when the nanowire is accumulated (dashed line), relative to when the charge carriers are depleted (solid line).

Using the known, designed value of inductance L, and having measured the resonance frequency with the carriers depleted and accumulated, ${f_0}^{\mathrm{depl/acc}}$, the gate capacitance C_G is obtained from a set of two equations:

$$ {f_0}^{\mathrm{depl}} = \frac{1}{2\pi\sqrt{LC}}, \quad {f_0}^{\mathrm{acc}} = \frac{1}{2\pi\sqrt{L(C+C_G)}}. \tag{1} $$

Here C is the capacitance of the resonator, including the self-capacitance of the inductor and parasitic capacitance of the bondwires and the source contact. Equivalently,

$$ \begin{aligned} C_G &= \frac{1}{(2\pi {f_0}^{\mathrm{depl}})^2 L} - \frac{1}{(2\pi {f_0}^{\mathrm{acc}})^2 L} \\ &\approx -\frac{\Delta f_0}{2\pi^2 ({f_0}^{\mathrm{depl}})^3 L}, \end{aligned} \tag{2} $$

where the last approximation assumes a small resonator shift $\Delta f_0 \ll f_0$.

With the resonator attached to the device gate, the capacitance measurement is performed similarly. In this case, either one or both of the barrier gate voltages $V_{L/R}$ must be set to accumulate electrons to provide a low-impedance shunt to rf ground. The two configurations of connecting the resonator (to the device source or gate) measure slightly different quantities, and are subject to different constraints.

First, the rf resonance frequency is affected by capacitance between the attached contact (source or gate) and any rf ground. This includes, e.g., other gates or a conducting substrate. If gating of the active part of the device also influences other relevant parts of the device (e.g., the substrate), the capacitance method becomes unreliable. In the validation experiment we ensure that is not the case by using a highly resistive Si substrate.

Second, the channel tuned by V_G may be coupled capacitively to multiple gates. Thereby, resonators attached to the device lead or gate will measure different capacitances. If the resonator is connected to the tuned gate, it will only detect capacitance changes between the channel and the tuned gate. Meanwhile, a measurement with the resonator connected to the source lead detects capacitance changes between the carriers accumulated in the channel and *all* gates. Depending on the purpose of the measurement, either one or both of these implementations may be desirable.

In particular, if a number of gates is coupled to the same segment of the conducting channel, the resonators attached to the gates can be employed to quantify their relative capacitance. However, we note that in those cases the conducting channel itself often contributes to the screening of the gate. Consequently, the capacitances effectively change depending on, e.g., whether the channel is galvanically connected to the leads, depleted, or if quantum dots are formed. In our devices the capacitance between the channel and the gate dominates over capacitances between the channel and other elements of the device.

Third, attaching the resonator to the device source enables using it for measuring the capacitance of multiple connected devices, since dc gate voltages can be applied separately, and used to select between the devices. However, if the device yield is low, this may be undesirable, as a single faulty device may introduce a rf short to ground and render the resonator unusable.

Finally, in case the resonator is attached to the device source, it can be repurposed for rf conductance measurements [5,27,28]. When the source-drain resistance is finite, it introduces dissipation in the resonant circuit, mapping the channel conductance to the internal quality factor of the resonator.

In the validation experiment (Sec. III) we measure the capacitance of three InSb devices: for two of them, we

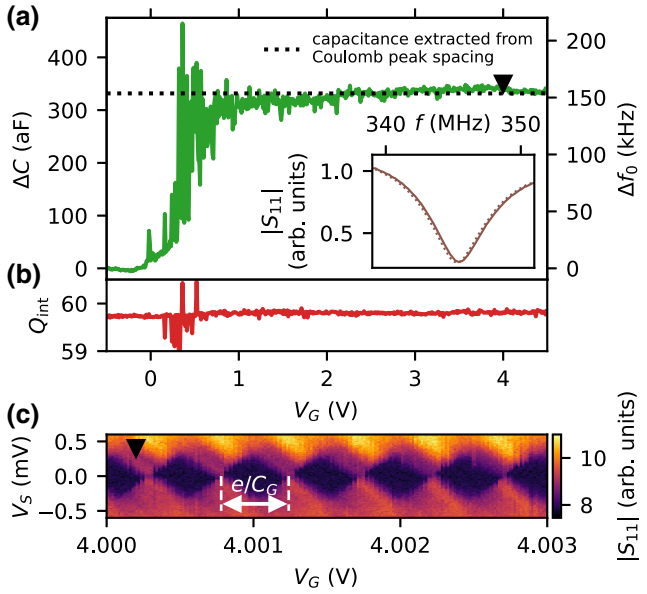

FIG. 2. (a) Frequency shift, Δf, and a corresponding capacitance change, ΔC, as a function of the plunger gate voltage V_G for a 2-μm-long InSb device. The dotted line indicates the gate capacitance extracted from the Coulomb blockade measurement at $V_G = 4$ V, indicated with a triangular marker. Inset: $|S_{11}|$ versus frequency at $V_G = -0.5$ V (solid line) and 4 V (dotted line). (b) Internal quality factor Q_{int} of the resonator. (c) rf Coulomb diamonds measurement. The periodicity of the Coulomb blockade provides an independent measure of the gate capacitance.

attach the resonator to the source contact, and for the last one, we attach the resonator to the gate. In a noise characterization experiment (Sec. IV) we measure the resonator attached to the source contact of an InAs device.

III. VALIDATION

To verify that the rf capacitance measurement provides quantitatively accurate results, we compare the capacitances extracted from the resonator shift and from the periodicity of the Coulomb blockade for InSb devices with 80, 500, and 2000 nm gate widths. An example of such a comparison is shown in Fig. 2 for a device with 2-μm-wide bottom gate.

First, we pinch off a section of the nanowire with a gate voltage V_R and accumulate with V_L, thereby connecting the nanowire bulk to the source contact and disconnecting it from the drain. Next, we measure the reflection S_{11} from the rf resonator as a function of the drive frequency f and gate voltage V_G. For each V_G, we fit the resonator response (see Appendices A–C). The extracted resonance frequency change, Δf_0, capacitance change, ΔC, and resonator internal quality factor, Q_{int}, are plotted in Figs. 2(a) and 2(b).

The resonance frequency is nearly constant below about $V_G \approx -0.2$ V. The resonator shift gradually increases when increasing V_G from -0.2 to 1 V, and saturates above $V_G \approx 1$ V. The total shift of about 150 kHz corresponds to an increase in capacitance of $C_G = 334.8 \pm 1.0$ aF, which we identify as a gate-wire capacitance. The range over which the capacitance gradually increases is consistent with the range over which the gate voltage V_G tunes the channel from fully closed to fully open in a lock-in conductance measurement (cf. Sec. V B and Fig. 5 therein). We attribute the peaks in the intermediate range of V_G to the quantum capacitance of unintentional quantum dots formed in the disordered potential in the wire. Panel (b) demonstrates the change of the resonator internal quality factor Q_{int} as a function of the gate voltage. The inset of Fig. 2(a) illustrates a small change in the resonance frequency compared to the resonator linewidth. Except for the random error, we expect the main source of the potential systematic error to be up to about 1.5% due to kinetic inductance of the 200-nm-thick superconducting film forming the superconducting inductor.

To independently measure the gate capacitance with a different method, we form a quantum dot by setting the gate voltages $V_{L,R} \sim 150$ mV to a tunneling regime, and $V_G \approx 4$ V. Coulomb diamonds versus V_G and V_S are measured by means of rf conductance [5,27,28], using the same resonator that was used for the direct capacitance measurement [Fig. 2(c)]. The spacing between the Coulomb peaks ΔV_G corresponds to the gate voltage change required to add a single electron to a quantum dot [29], and is related to the gate capacitance via $\Delta V_G = e/C_G$. This measurement yields capacitance $C_G = 331.7 \pm 7.8$ aF, in good agreement with the value extracted from the resonator shift.

The same measurement is repeated for two other InSb nanowire devices, with gate widths of 80 and 500 nm. Table I lists the capacitances extracted by both methods for all three devices, and supporting data are presented in Appendix E. In all cases we find that the two methods are in good agreement.

IV. SENSITIVITY

Next, we investigate the sensitivity of the capacitance measurement. To maximize the sensitivity, it is

TABLE I. Comparison of gate capacitance extracted from the Coulomb blockade and resonator shift.

Gate size (nm)	Resonator placement	Capacitance (aF)	
		Resonator shift	Coulomb blockade
80	Source	31.7 ± 0.6	27.5 ± 1.7
500	Gate	115.1 ± 0.2	114.4 ± 3.7
2000	Source	334.8 ± 1.0	331.7 ± 7.8

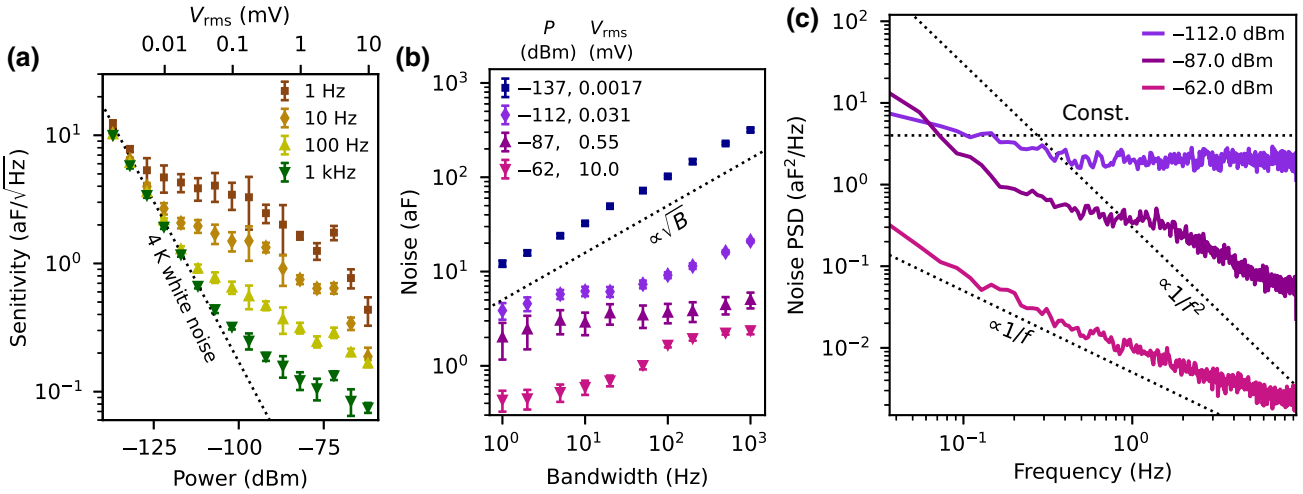

FIG. 3. (a) The measured sensitivity of the capacitance measurement. The dotted line indicates the sensitivity limit due to the amplifier noise ($T_{\text{noise}} \approx 4$ K). (b) The standard deviation of the gate capacitance measurement versus the vector network analyzer bandwidth. The dotted line indicates the scaling of the noise $\propto \sqrt{B}$, expected for white noise such as Johnson-Nyquist noise. (c) The capacitance noise power spectrum (PSD) for a measurement bandwidth of 50 Hz.

beneficial to perform the measurement only near the resonance frequency. With an analytical model of the resonator and assuming fixed quality factors, the amplitude and phase measurement at fixed frequency allows us to determine the frequency shift and, therefore, the added capacitance (Appendices C and D).

We characterize the sensitivity of the capacitance measurement on an InAs nanowire device with a 340-nm-wide gate wrapped around the nanowire. The inductor ($L = 730$ nH) is attached to the source lead of the device. The resonator has a resonant frequency $f_0 = 312.81$ MHz, an internal quality factor of $Q_{\text{int}} = 488$, and an external quality factor of $Q_{\text{ext}} = 134$.

We acquire time traces of the signal reflected from the resonator at a fixed frequency $f = 313.21$ MHz, first with the gate voltage V_G set to fully open, and then to fully closed. This procedure is repeated for various vector network analyzer bandwidths B and drive powers, while maintaining a fixed total 4.5 min length of time traces. The fixed duration of several minutes is chosen in order to expose the setup to detrimental influence of the device drift and low-frequency noise, and to obtain fair values of a noise level applicable to a real use case. We define the SNR for distinguishing the open and closed cases as

$$\text{SNR} = \left| \frac{{S_{11}}^{\text{open}} - {S_{11}}^{\text{closed}}}{(\sigma_{11}^{\text{open}} + \sigma_{11}^{\text{closed}})/2} \right|, \tag{3}$$

where ${S_{11}}^{\text{open/closed}}$ and $\sigma_{11}^{\text{open/closed}}$ are the mean and standard deviation of the measured complex reflection coefficient for the gate being open and closed. Based on the SNR we define the noise and the sensitivity of the capacitance measurement as $N = \Delta C/\text{SNR}$ and $s = \Delta C/(\text{SNR} \times \sqrt{B})$, respectively [30].

Figure 3 shows the measured sensitivity and noise for various measurement bandwidths and excitation powers. Panel (a) demonstrates that the measurement sensitivity improves with increased rf excitation power, where the top axis represents the corresponding root-mean-square (rms) voltage V_{rms} on the contact attached to the resonator. The low-power sensitivity is independent from the measurement bandwidth. As power increases, the sensitivity becomes increasingly more bandwidth dependent with the lowest values corresponding to the highest used bandwidth of 1 kHz. In Fig. 3(a) we indicate the sensitivity expected for about 4 K thermal (white) noise (Appendix A), which approximates the expected noise level for the used cryogenic amplifier (Cosmic Microwave CITLF2, nominal noise temperature 1.6 K) mounted at the 4 K plate of the dilution refrigerator (actual temperature 3.4 K). For 1 kHz bandwidth and below −100 dBm drive power, the measured sensitivity matches the 4 K noise limitation. When the drive power is increased further, the sensitivity falls short of the limit more significantly. As the bandwidth is reduced, the sensitivity exceeds the 4 K limit at lower power—for 1 Hz bandwidth, deviation from the amplifier limit occurs already at about −125 dBm. Furthermore, a plateaulike region in sensitivity appears at 1 Hz, between about −110 and −100 dBm.

To gain insight into the absolute precision of the capacitance measurement, we plot the absolute noise level in Fig. 3(b). At the lowest drive power (−137 dBm) the noise scales as $\sqrt{B}$, indicating that white amplifier and thermal noise are dominating. As the power increases, the noise appears to saturate at a few-attofarad level. At −87 dBm

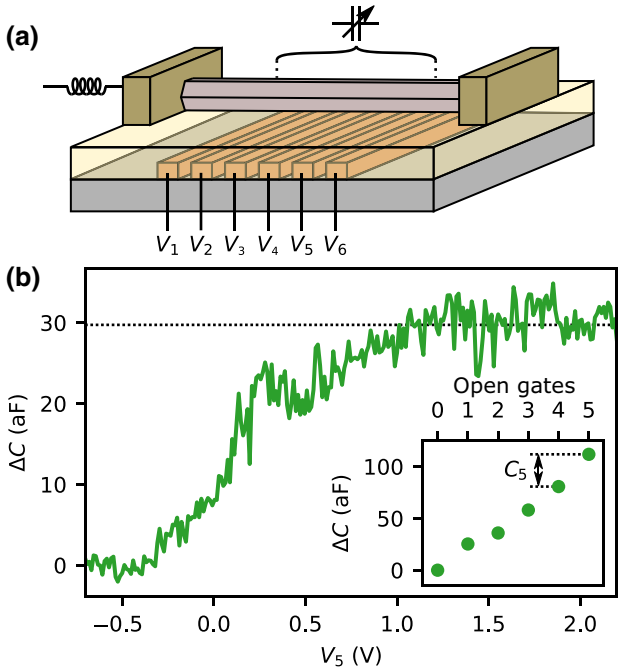

FIG. 4. (a) A schematic of the InSb nanowire device with six parallel 80-nm-wide bottom gates, spaced by 60 nm. The coil symbol indicates the drain contact connected to a rf resonator. (b) Capacitance added to the circuit as a function of the voltage V_5 on one of the gates. Inset: values of the added capacitance with 0 to 5 of the bottom gates in the open state. Error bars in the measured capacitance values are smaller than the marker size.

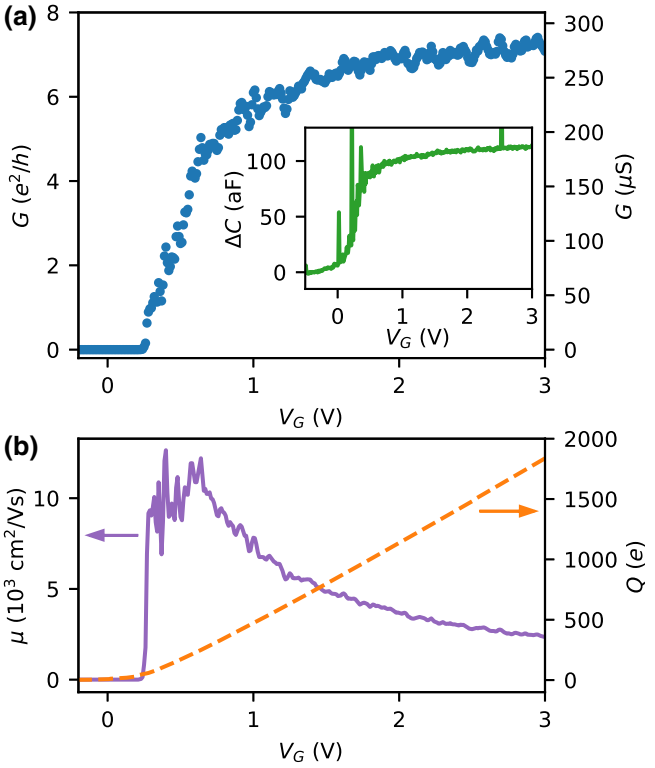

FIG. 5. (a) Conductance G as a function of the gate voltage V_G in an InSb nanowire device with 500-nm-wide bottom gate. Inset: added capacitance ΔC as a function of the gate voltage V_G. (b) Mobility of the nanowire device and charge in the conductive channel versus the gate voltage V_G.

the bandwidth change from 1 kHz to 1 Hz only reduces the noise from 4 to 2 aF. At even higher power (−62 dBm) the noise decreases further, reaching the lowest value of 0.45 aF for 1 Hz bandwidth.

To identify an origin of the plateaulike region in low-bandwidth sensitivity and the apparent saturation of noise at a few-attofarad level, we measure the capacitance noise spectra at 50 Hz bandwidth and for −87 dBm power [Fig. 3(c)]. At low drive power (−112 dBm) we find that the noise is predominantly white, while at the highest power (−62 dBm) its spectrum is close to $1/f$. The onset of the $1/f$ noise explains why the sensitivity is above the 4 K limit at low bandwidths and high powers. However, for intermediate drive power, the noise exhibits a peculiar spectrum: it is white in the range between 0.5 and 1 Hz, and close to $1/f^2$ below and above that range. Direct inspection of the time traces used to calculate noise (see Fig. 8 in Appendix E) reveals that this noise spectrum is due to telegraph noise from two two-level systems, characterized by very different switching rates. Each contributes a Lorentzian component to the noise spectrum.

We speculate that these two-level systems are individual impurities in the vicinity of the nanowire device that are activated only at a specific gate voltage. At low drive powers the influence of impurities is not resolvable due to the white noise. At intermediate power their influence is resolvable, leading to the apparent saturation of noise and plateaulike features. For high power, the impurities contribute less to the capacitance because charging of the impurity with a fixed charge Q_{impurity} contributes relatively less to the capacitance for larger rms voltage excitation—about $Q_{\text{impurity}}/V_{\text{rms}}$. While we expect the white and $1/f$ noise to be generic to the implementations of the rf capacitance measurements with a resonator, the telegraph noise is specific to the device we used for the sensitivity benchmarking.

Finally, we estimate the expected sensitivity of the capacitance measurements for several implementations of rf resonators and noise temperatures (Table II), assuming that the dominant contribution to noise is white noise. The first entry represents a slight improvement that could be expected in a setup identical to ours at moderate drive powers, thanks to an increase in the resonator internal and external quality factors. The second entry shows typical sensitivities that could be achieved using the resonator design (i.e., 50 Ω, superconducting CPW resonator) and the amplification chain widely used for readout of superconducting qubits [1]. The third entry indicates the

TABLE II. Summary of the estimated sensitivities for several realizations of the rf resonant circuits and amplifiers, assuming that the performance is limited by Johnson-Nyquist noise. The last entry illustrates the capacitance performance of a low-noise capacitance bridge. SC, superconducting; CPW, coplanar wave guide; surface mount, limped-element resonator made of off-the-shelf surface-mount components; HEMT, high-electron-mobility transistor; TWPA, traveling-wave parametric amplifier; SQUID, superconducting quantum interference device.

Resonator type	Amplifier	f_0 (GHz)	Z_{char} (Ω)	Q_{int}	Q_{ext}	P (dBm)	V_{rms} (mV)	T_{noise} (K)	S_C (zF/$\sqrt{\text{Hz}}$)	Source
SC spiral inductors	4 K HEMT	0.35	1000	500	300	−100	0.14	4	80	This work[a]
SC CPW resonator	TWPA	5	50	10^4	10^3	−120	6.7×10^{-3}	0.6	60	Ref. [3]
Surface mount cryogenic	Low-noise SQUID	0.196	275	30	30	−80	0.20	0.6	110	Ref. [4]
Surface mount, room temperature	300 K HEMT	0.26	650	30	150	−40	40	300	40	Appendix E[b]
Capacitance bridge	n/a	n/a	n/a	n/a	n/a	n/a	20	n/a	2200	Ref. [9]

[a] Typical values from among several spiral inductor chips and nanowire devices.
[b] Self-resonance of a 1 μH surface-mount inductor (Coilcraft, 1008CS-102X_E_).

possible performance that can be achieved using the self-resonance of off-the-shelf surface-mount inductors at cryogenic temperatures and state-of-the-art amplification [4]. In the fourth entry, we estimate that similar sensitivity can be achieved at room temperature, with the effective rms voltage on the device contact comparable to the magnitude of the voltage excitation in capacitance bridges. The last entry presents, as a reference, the performance of a low-noise capacitance bridge.

We note that these estimates may be expected to be valid only in a limited range of bandwidths. For low bandwidths, the sensitivity estimates may likely break down due to intrinsic properties of the device under study, or $1/f$ noise, as is the case in our experiment. For bandwidths $B \sim f_0 \times Q_{\text{int}}$ and higher, the estimates break down because the measurement time is comparable to the time for the reflection to reach a steady state.

V. EXAMPLES OF APPLICATION

In this section we list several use cases for the capacitance measurement with rf resonators. We demonstrate how a single resonator can be used to measure capacitance of multiple gates (Sec. V A), and to supplement conductance measurements in extracting the mobility of an individual nanowire (Sec. V B). In Sec. V C we list a few quantum-mechanical phenomena that affect the electronic compressibility, and thereby can be studied with a sufficiently sensitive capacitance measurement. Section V D proposes an implementation of the rf resonator on the needle of a micromanipulator for rapid capacitance measurements in a probe station.

A. Capacitance of multiple gates measured with a single resonator

To demonstrate that a single rf resonator attached to a lead can be used to measure multiple gates, we focus on an InSb nanowire device with six 80-nm-wide parallel bottom gates [Fig. 4(a)], labeled V_1 through V_6. The rf resonator is only attached to a single lead, and yet we use it to measure the capacitance of gates 1 through 5. We start with all gates at large negative voltages. The gate voltage V_1 is then gradually increased, while measuring the resonance frequency of the resonator. When the measured value of the capacitance saturates, we assign the corresponding value to the first gate, and proceed to sweeping the next gate voltage. The measured change in the capacitance in a sweep of the gate voltage V_5 is presented in Fig. 4(b). The inset of Fig. 4(b) illustrates the saturation values of capacitance with the first N gates opened. In this configuration it is not possible to measure the capacitance of the sixth gate V_6. As soon as it accumulates carriers, the rf circuit becomes terminated with a low impedance of the drain lead and the resonance feature in a reflection measurement vanishes.

We suggest that the capability of measuring capacitance of multiple small gates with a single resonator may be applicable in the development and characterization of multigate structures, e.g., arrays of quantum dots for spin qubits [31–33].

B. Mobility

Next, we demonstrate the possibility of using the rf-resonator-based capacitance measurement to complement dc conductance measurements in determining the mobility of individual submicrometer devices. Low-frequency *C-V* measurements of such devices are very challenging due to the small values of capacitance. This is usually resolved by measuring the capacitance of multiple nominally identical devices connected in parallel, or by relying on finite-element simulations. These approaches may obscure the variation between individual devices or lead to systematic errors.

In our demonstration, we focus on an individual InSb nanowire with a 500-nm-wide bottom gate [cf. Fig. 1(a)]. We start by measuring the gate capacitance as described in Sec. II (inset of Fig. 5). Afterwards, we measure the conductance across the device versus the gate voltage V_G with all other gates open, using a two-terminal lock-in measurement with a 3 mVrms excitation voltage, corrected for resistances in the filtered lines of the cryostat [Fig. 5(a)].

We integrate numerically the gate capacitance versus V_G to calculate the total charge Q in the conductive channel,

$$Q(V_G) = \int_{-0.5V}^{V_G} \Delta C(\tilde{V}_G)\mathrm{d}\tilde{V}_G, \tag{4}$$

where e is the electron charge, and the lower integration limit of -0.5 V is chosen to be well below the pinch-off voltage. Finally, we calculate the mobility $\mu(V_G) = l^2 G(V_G)/Q(V_G)$, where $l = 500$ nm is the nanowire length and G is the measured conductance. The calculated charge and mobility are plotted in Fig. 5(b). We find a peak mobility of $\mu \approx 1.2 \times 10^4$ cm^2/Vs. This value is somewhat lower than other measurements on nanowires grown by the same process [23]. We expect that this is due to the use of the field-effect model [34] to fit the data in Ref. [23], and possibly due to more involved fabrication of the devices for our experiment. The field-effect model assumes gate-independent mobility and saturation of the pinch-off curve to additional in-line (e.g., contact) resistance, yielding higher values of the extracted mobility. Using the field-effect model, we extract a mobility of $\mu_{\mathrm{FE}} = 2.3 \times 10^4$ cm^2/Vs (Appendix E).

C. Electronic compressibility in mesoscopic devices

In multiple solid-state physics phenomena, the charging of the mesoscopic system is not only affected by the geometrical capacitance of the device. Properties such as the electronic band structure and electron-electron interaction affect the electronic compressibility, resulting in a nonclassical contribution to the device capacitance. To date, measurements of the bulk electronic compressibility were mostly performed by means of capacitance bridges [21,35] or the electric field penetration technique [36–38]. Quantum effects of one-dimensional and mesoscopic devices are at the very limit of what is possible to measure with these methods. With subattofarad noise, for the same or smaller excitation amplitudes, a number of phenomena can be further explored.

Electronic compressibility is a hugely informative quantity in topics such as Luttinger liquids [21] and the quantum Hall regime (in all its flavors) [39,40]. Jarratt *et al.* [22] showed the ability to measure the van Hove singularities in a narrow GaAs quantum point contact using a resonator, demonstrating that compressibility measurements can give insight into the band structure of one-dimensional systems.

Compressibility divergence can indicate closing and reopening of the bulk gap. Compressibility measures the properties of the bulk directly, and does not rely on local probes, making it a uniquely good quantity to investigate topological phase transitions [41], including the case of topological superconducting phase transitions [42].

D. Implementation on a probe needle

As quantified in Table II, subattofarad sensitivities can be achieved using low-Q rf resonators. In particular, LC resonators constructed from surface-mount components are commonly used for state-of-the-art charge and spin readout [4,43–45]. These realizations use the self-resonance of the surface-mount inductor, and supplement it with additional capacitances to adjust the resonance frequency and characteristic impedance. While the referenced uses are demonstrated at cryogenic temperatures, these resonant circuits perform comparably well at room temperature (Appendix E).

This suggests a possible realization of a rf resonator in the form of a needle probe of a micromanipulator, or a scanning probe microscope. The needle could either make galvanic connection with the contact on the device, or approach the surface of the characterized material [46]. The surrounding environment would affect both the resonance frequency and quality factor as such a probe makes contact with the device, but lack of strict requirements on the resonance frequency and the quality factor render such changes mostly irrelevant in practical use cases. Thereby, the capacitance measurement method is suitable for the purpose of rapid screening of devices on a large scale.

VI. SUMMARY

To summarize, we validate a method of measuring capacitance of micro- and nanoscale devices by means of rf resonators. The method is characterized by the sensitivity reaching values as low as 75 zF/$\sqrt{\mathrm{Hz}}$ and noise below 1 aF for moderate integration times. It is suitable for applications at both room temperature and cryogenic temperatures, including dilution refrigerators. It is also suitable for measuring multiple gate capacitances with a single resonator, reducing the reliance on finite-element simulations for mobility measurements. Finally, we propose that the rf capacitance measurements can detect the quantum contribution to bulk capacitance in mesoscopic devices and can be implemented on the needle of a probe station with a micromanipulator. Raw data, analysis code, and scripts for plotting the figures for this publication are available from Zenodo [47].

ACKNOWLEDGMENTS

We thank John Watson and Gijs de Lange for valuable comments and suggestions. This work is supported

by the Netherlands Organization for Scientific Research (NWO), Microsoft Quantum Lab Delft, Quantum Materials Lab Copenhagen, and Quantum Lab Sydney. F.K.M. acknowledges support from NWO under a Veni grant (VI.Veni.202.034).

F.K.M. and J.V.K. envisioned the experiment. L.H., D.J., and J.W. fabricated the nanowire devices. F.K.M. performed the experiment and the data analysis. D.J. and C.P. provided reference data on CPW resonators. G.B., S.G., and E.P.A.M.B. grew the InSb nanowires. Y.L. and P.K. grew the InAs nanowires. L.K. supervised the project. F.K.M. wrote the manuscript with input from L.H., D.J., J.W., C.P., Y.L., L.K., and J.V.K.

F.K.M. and J.V.K. are named as inventors on the pending patent application, PCT Application No. PCT/EP2020/061956, which concerns the method described in this article.

APPENDIX A: BASIC RESONATOR MODEL AND SENSITIVITY ESTIMATE

The starting point for modeling the resonator is a series *RLC* circuit coupled to a $Z_0 = 50\Omega$ transmission line [48]. The impedance of such a resonator is

$$Z = R + 2\pi i f L + \frac{1}{2\pi i f C} \overset{\Delta f \ll f_0}{\approx} Q_{\text{ext}} Z_0 \left(\frac{1}{Q_{\text{int}}} + i \frac{2\Delta f}{f_0} \right), \tag{A1}$$

where R, L, and C are resistance, inductance, and capacitance of the *RLC* circuit, respectively; $Q_{\text{ext}} = Z_{\text{char}}/Z_0$ is the external quality factor; $Q_{\text{int}} = Z_{\text{char}}/R$ is the internal quality factor; $Q = ({Q_{\text{ext}}}^{-1} + {Q_{\text{int}}}^{-1})^{-1}$ is the total quality factor; $Z_{\text{char}} = \sqrt{L/C}$ is the characteristic impedance of the resonator; $f_0 = 1/(2\pi\sqrt{LC})$ is the resonance frequency; f is the probe frequency; and $\Delta f = f - f_0$.

The reflection coefficient of the resonator is thereby

$$S_{11} = \frac{Z - Z_0}{Z + Z_0} = 1 - \frac{2Q{Q_{\text{ext}}}^{-1}}{1 + 2iQ(f - f_0)/f_0}. \tag{A2}$$

Maximum sensitivity to small changes in the resonator frequency is achieved by measuring exactly on resonance

$$\left. \frac{dS_{11}}{df_0} \right|_{f = f_0} = -4i \frac{Q^2 {Q_{\text{ext}}}^{-1}}{f_0}. \tag{A3}$$

In a lumped-element resonator model this corresponds to a maximum sensitivity to capacitance changes of

$$\left. \frac{dS_{11}}{dC} \right|_{f = f_0} = 4\pi i \frac{Q^2}{Q_{\text{ext}}} f_0 Z_{\text{char}}. \tag{A4}$$

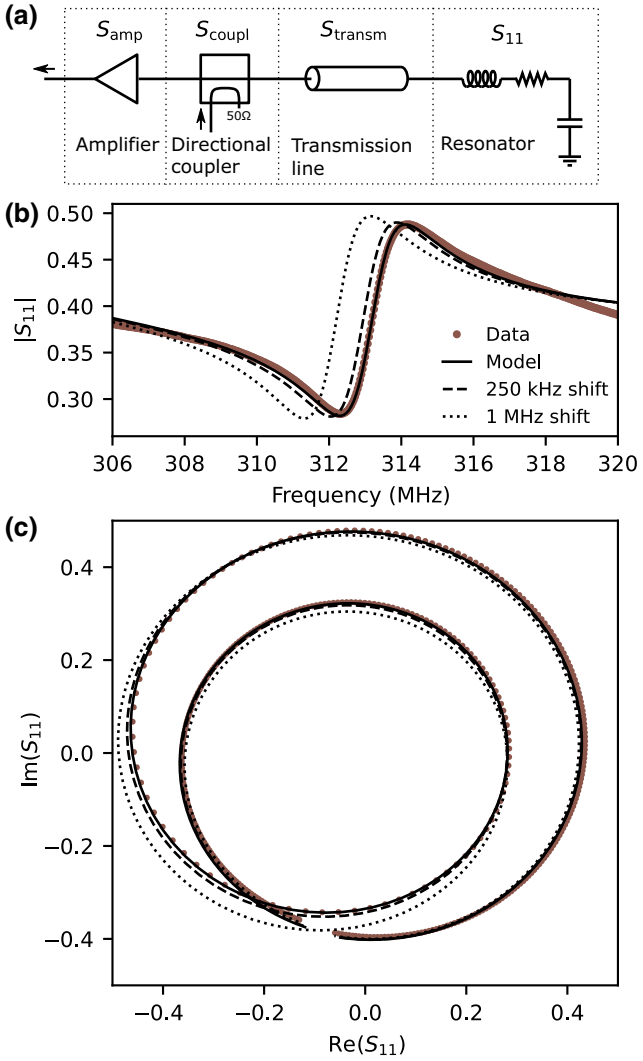

FIG. 6. (a) Circuit schematics employed to model the resonance asymmetry of the resonator used for characterization of the performance in Sec. IV. (b) Absolute value of S_{11} and (c) parametric plot of the real and complex parts. The solid line indicates the fit of Eq. (C1) to the data. The dashed and dotted lines indicate the predicted signal in the cases when the resonance frequency is lowered by 250 kHz and 1 MHz, respectively.

For a drive amplitude A and noise voltage variance σ_v^2 per unit of bandwidth, the sensitivity is given by

$$S_C = \frac{\sigma_v}{A} \left| \frac{dS_{11}}{dC} \right|^{-1}. \tag{A5}$$

APPENDIX B: ORIGIN OF THE RESONANCE ASYMMETRY

In the study we generally find asymmetric line shapes of the rf resonances [cf. Fig. 6(b)], with the asymmetry typically being more pronounced for high internal quality factors. In the hanger geometry an asymmetry is usually attributed to the mismatch between the impedance of the

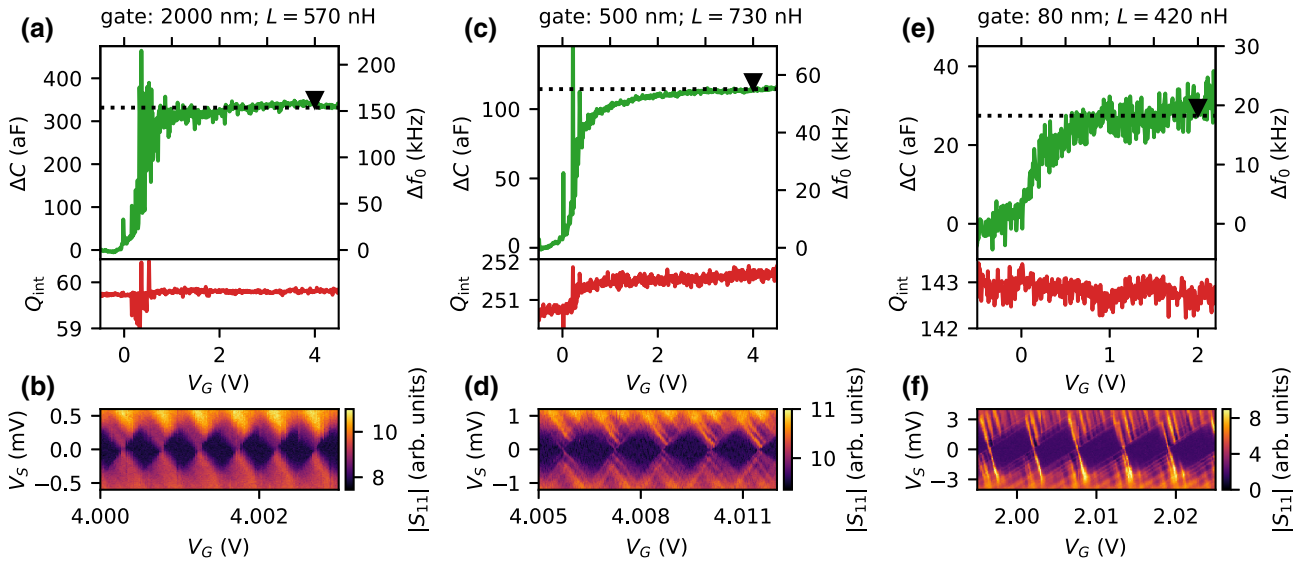

FIG. 7. (a),(c),(e) The *C*-*V* measurements using rf resonators for the three InSb devices with gate widths of 2000, 500, and 80 nm. Bottom panels present internal quality factors of the resonators as a function of the gate voltage V_G. (b),(d),(f) rf-conductance measurements of Coulomb diamonds for quantum dots formed in nanowire devices.

input and output transmission lines [49]; however, such an interpretation has no physical justification in a reflection measurement. One approach in reflectometry is therefore to neglect the extraction of the frequency shift and quality factor from the data. Another approach is to use additional phenomenological factors to account for asymmetry [50]. The phenomenological approach leads to correct extraction of the resonance frequency, but introduces systematic error in the extraction of the internal and external quality factors. Here, we introduce an approach utilizing a physically motivated model that captures the resonance asymmetry.

Our model considers a cryogenic circuit depicted in Fig. 6(a), consisting of the resonator itself, a directional coupler (characterized by a coupling parameter γ), a connecting transmission line (length l and microwave propagation speed c), and an amplifier. We describe each of these components using scattering matrices:

$$S_{\text{coupl}} = \begin{pmatrix} 0 & \sqrt{1-\gamma^2} & i\gamma & 0 \\ \sqrt{1-\gamma^2} & 0 & 0 & i\gamma \\ i\gamma & 0 & 0 & \sqrt{1-\gamma^2} \\ 0 & i\gamma & \sqrt{1-\gamma^2} & 0 \end{pmatrix}, \tag{B1}$$

$$S_{\text{transm}} = \begin{pmatrix} 0 & e^{-2\pi i f l/c} \\ e^{-2\pi i f l/c} & 0 \end{pmatrix}, \tag{B2}$$

$$S_{\text{amp}} = \begin{pmatrix} \sqrt{1-\alpha^2}e^{i\phi} & \alpha \\ \alpha & \sqrt{1-\alpha^2}e^{i\phi} \end{pmatrix}. \tag{B3}$$

Here the amplifier is treated as a partially reflective mirror with a transmission coefficient α that introduces a phase shift ϕ to the reflected signal. The reflection coefficient of the resonator S_{11} is given by Eq. (A2). Two effective mirrors, the resonator, and the amplifier form a low-Q cavity that modulates the transmission through the circuit from the coupled port of the directional couplet to the output of the amplifier. The modulation leads to the resonance asymmetry, and in some cases can even turn the resonance dip into a peak, through the following mechanism.

The cavity formed between the resonator and the amplifier reduces the output signal, except on resonance (i.e., when on the round trip between the amplifier and the resonator the microwaves acquire a phase that is a multiple of 2π). This leads to the oscillating background in the reflection measurement. If the resonator is undercoupled ($Q_{\text{int}} > Q_{\text{ext}}$), near resonance frequency f_0, the phase of S_{11} rapidly wraps by 2π. Therefore, there must exist a frequency, close to f_0, for which the round trip is an exact multiple of 2π, resulting in an increase of the transmission through the cavity formed by an amplifier, and leading to an asymmetry.

Analytically, we solve the set of linear equations

$$\vec{V}_i^{\text{out}} = S_i \times \vec{V}_i^{\text{in}}, \tag{B4}$$

given by the scattering matrices S_i [Eqs. (A2), (B1), (B2), and (B3)], relating the microwave amplitude and phase at the inputs ($\vec{V}_i^{\text{in}}$) and outputs ($\vec{V}_i^{\text{out}}$) of each component of the circuit. In the solution we assume that the microwave drive is applied only to the coupled port of the directional coupler, and that the drive is zero on the isolated port and output of the amplifier and mirror. We find the transmission from the coupled input of the directional coupler to

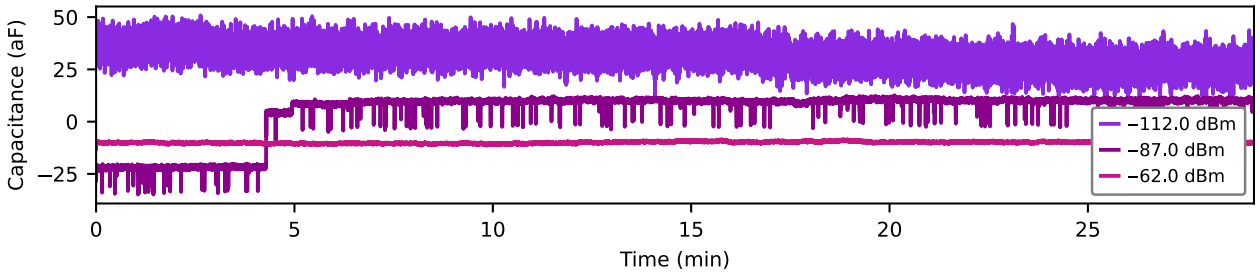

FIG. 8. Time traces of the measured capacitance for the depleted InAs nanowire device, used to calculate the noise power spectrum density in Fig. 3(c). Time traces are offset vertically for clarity.

the amplifier:

$$\tilde{S}_{11} = \frac{i\gamma\alpha\sqrt{1-\gamma^2}e^{-4\pi fli/c+i\phi}S_{11}}{1-\sqrt{1-\alpha^2}(1-\gamma^2)e^{-4\pi fli/c+i\phi}S_{11}}. \qquad \text{(B5)}$$

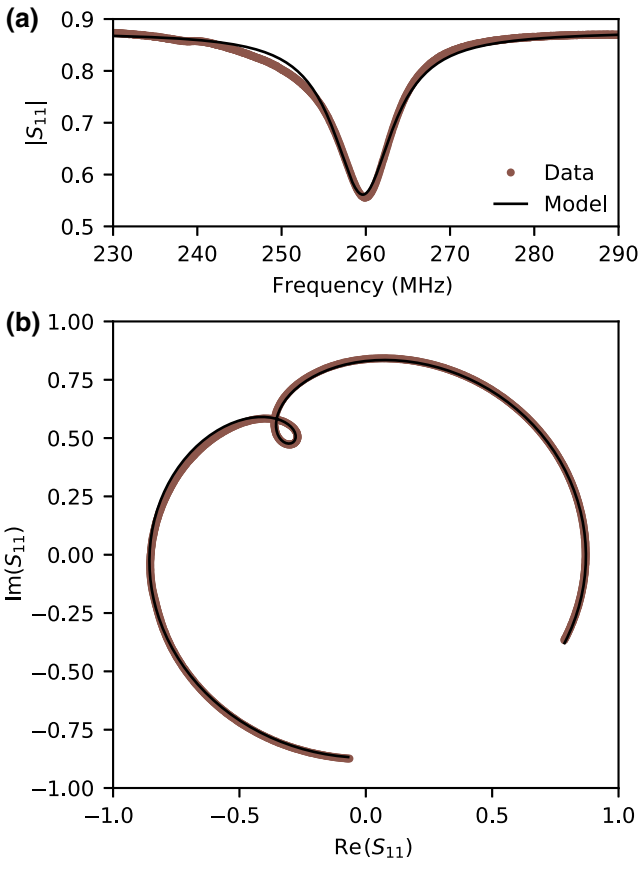

FIG. 9. (a) Magnitude of the reflection around the self-resonance frequency of the surface-mount inductor. (b) Parametric plot of the real and imaginary parts of the reflection around the self-resonance frequency. Black lines indicate fits to the data.

APPENDIX C: RESONATOR FITTING

In a final fit to the data, we include additional prefactors to modify Eq. (B5),

$$\tilde{\tilde{S}}_{11} = A\left(1+B\frac{f-f_0}{f_0}\right)\times e^{-i\zeta+i\beta(f-f_0)}\times\tilde{S}_{11}, \qquad \text{(C1)}$$

and record the optimal parameters. The term $A[1+B(f-f_0)/f_0]$ phenomenologically accounts for a frequency-dependent attenuation and amplification, while $e^{-i\zeta+i\beta(f-f_0)}$ accounts for the phase shift accumulated during propagation through the transmission lines. The A and B factors parameterize the background amplitude and slope, while ζ and β parameterize the global phase shift and phase winding.

In the fits we fix several of the parameters independently. The coupling coefficient $\gamma = 0.178$ (equivalently, 15 dB) is chosen according to the specification of the used Mini Circuits ZEDC-15-2B [51], and the reflection coefficient $\alpha = 0.398$ corresponds to an 8 dB return loss of the Cosmic Microwave CITLF2 HEMT cryogenic amplifier [52]. We set the value of $(2l/c)^{-1} = 111.4$ MHz based on the measurement of the reflection at 4 K, with no device mounted in the setup. The remaining parameters are optimized in the nonlinear fit. Figure 6 depicts the fit result for the resonator used to quantify sensitivity in Sec. IV.

APPENDIX D: FREQUENCY SHIFT FROM FIXED-FREQUENCY MEASUREMENT

To maximize the measurement sensitivity, it is optimal to perform a fixed-frequency measurement, near the resonance frequency, for which the reflection coefficient responds most strongly. To recover the frequency shift from such a fixed-frequency measurement, we perform a calibration resonator measurement (Fig. 6) and fit the analytical model [Eq. (C1)] to the data (Appendix C). We fix all of the parameters of the model, except for the resonance frequency f_0. In this way we are able to predict the expected reflection coefficient for different values of the resonance frequency (e.g., the dashed and dotted lines in Fig. 6).

Next, we measure the reflection at fixed frequency f versus the gate voltage. For each data point, we perform

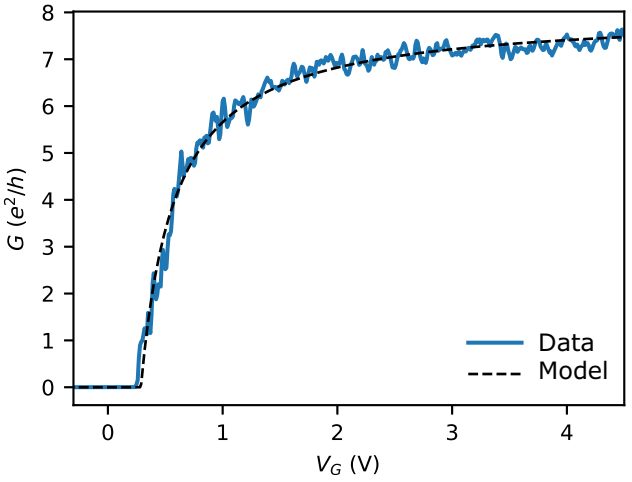

FIG. 10. Pinch-off curve of the 500 nm InSb device, used for extraction of mobility in Fig. 5.

numerical optimization to find f_0 that best matches the data, and identify the corresponding value as the resonance frequency at a given gate voltage.

In this work we assume that the internal quality factor Q_{int} of the resonator is not gate dependent, which is reasonably fulfilled [Fig. 2(b)]. We note that, since the reflection coefficient is complex valued, it could be used to infer two real-valued parameters simultaneously (f_0 and Q_{int}) via numerical optimization.

APPENDIX E: ADDITIONAL DATA SETS

In this appendix we present additional data sets, backing up the numerical values provided in the main text.

Figure 7 presents the C-V measurement for three devices listed in Table I. In the top panel of Fig. 7 the dashed line indicates the capacitance value extracted from the periodicity of the Coulomb blockade, and the triangular marker indicates the gate voltage V_G that is used for tuning the quantum dot.

Figure 8 presents time traces of the measured capacitance used to calculate the noise power spectra in Fig. 3(c). The data set for a -112 dBm drive power is dominated by white noise with a large magnitude, with a hint of a discrete jump at a time stamp of about 17 min. For a -87 dBm drive power, the SNR is sufficiently high to detect discrete changes in charge susceptibility from two-level systems in the vicinity of the device. At -62 dBm the large voltage excitation reduces the contribution of the individual impurities causing the telegraph noise.

Figure 9 presents the measurement of the self-resonance of the 1 μH surface-mount inductor (Coilcraft, 1008CS-102X_E_), together with a complex fit to the data. In these measurements no directional coupler or cryoamplifier is used; therefore, the data are fitted by Eq. (A2), with the prefactors listed in Appendix C. The parameters extracted from the fit are used in the final entry in Table II.

Figure 10 shows a fit of the field-effect model [34] to the pinch-off curve from Fig. 5. This fit yields the quoted value of mobility $\mu_{\text{FE}} = 2.3 \times 10^4$ cm^2/Vs.

[1] P. Krantz, M. Kjaergaard, F. Yan, T. P. Orlando, S. Gustavsson, and W. D. Oliver, A quantum engineer's guide to superconducting qubits, Appl. Phys. Rev. **6**, 021318 (2019).

[2] A. Chatterjee, P. Stevenson, S. De Franceschi, A. Morello, N. P. de Leon, and F. Kuemmeth, Semiconductor qubits in practice, Nat. Rev. Phys. **3**, 157 (2021).

[3] C. Macklin, K. O'Brien, D. Hover, M. Schwartz, V. Bolkhovsky, X. Zhang, W. Oliver, and I. Siddiqi, A near–quantum-limited Josephson traveling-wave parametric amplifier, Science **350**, 307 (2015).

[4] F. Schupp, F. Vigneau, Y. Wen, A. Mavalankar, J. Griffiths, G. Jones, I. Farrer, D. Ritchie, C. Smith, and L. Camenzind, *et al.*, Sensitive radiofrequency readout of quantum dots using an ultra-low-noise squid amplifier, J. Appl. Phys. **127**, 244503 (2020).

[5] R. Schoelkopf, P. Wahlgren, A. Kozhevnikov, P. Delsing, and D. Prober, The radio-frequency single-electron transistor (rf-set): A fast and ultrasensitive electrometer, Science **280**, 1238 (1998).

[6] F. Vigneau, F. Fedele, A. Chatterjee, D. Reilly, F. Kuemmeth, F. Gonzalez-Zalba, E. Laird, and N. Ares, Probing quantum devices with radio-frequency reflectometry, (2022), arXiv preprint ArXiv:2202.10516.

[7] O. Gunawan, L. Sekaric, A. Majumdar, M. Rooks, J. Appenzeller, J. W. Sleight, S. Guha, and W. Haensch, Measurement of carrier mobility in silicon nanowires, Nano Lett. **8**, 1566 (2008).

[8] E. C. Garnett, Y.-C. Tseng, D. R. Khanal, J. Wu, J. Bokor, and P. Yang, Dopant profiling and surface analysis of silicon nanowires using capacitance–voltage measurements, Nat. Nanotechnol. **4**, 311 (2009).

[9] Y.-C. Tseng and J. Bokor, Characterization of the junction capacitance of metal-semiconductor carbon nanotube Schottky contacts, Appl. Phys. Lett. **96**, 013103 (2010).

[10] Z. Ji, J. Gillbert, J. Zhang, and W. Zhang, in *2013 IEEE International Conference on Microelectronic Test Structures (ICMTS)* (IEEE, 2013), p. 64.

[11] K. Petersson, C. Smith, D. Anderson, P. Atkinson, G. Jones, and D. Ritchie, Charge and spin state readout of a double quantum dot coupled to a resonator, Nano Lett. **10**, 2789 (2010).

[12] J. Colless, A. Mahoney, J. Hornibrook, A. Doherty, H. Lu, A. Gossard, and D. Reilly, Dispersive Readout of a Few-Electron Double Quantum Dot with Fast rf Gate Sensors, Phys. Rev. Lett. **110**, 046805 (2013).

[13] M. Gonzalez-Zalba, S. Barraud, A. Ferguson, and A. Betz, Probing the limits of gate-based charge sensing, Nat. Commun. **6**, 6084 (2015).

[14] M. Urdampilleta, A. Chatterjee, C. C. Lo, T. Kobayashi, J. Mansir, S. Barraud, A. C. Betz, S. Rogge, M. F. Gonzalez-Zalba, and J. J. Morton, Charge dynamics and

spin blockade in a hybrid double quantum dot in silicon, Phys. Rev. X **5**, 031024 (2015).

[15] D. De Jong, J. Van Veen, L. Binci, A. Singh, P. Krogstrup, L. P. Kouwenhoven, W. Pfaff, and J. D. Watson, Rapid Detection of Coherent Tunneling in an InAs Nanowire Quantum Dot through Dispersive Gate Sensing, Phys. Rev. Appl. **11**, 044061 (2019).

[16] P. Pakkiam, A. Timofeev, M. House, M. Hogg, T. Kobayashi, M. Koch, S. Rogge, and M. Y. Simmons, Single-shot single-gate rf spin readout in silicon, Phys. Rev. X **8**, 041032 (2018).

[17] A. West, B. Hensen, A. Jouan, T. Tanttu, C.-H. Yang, A. Rossi, M. F. Gonzalez-Zalba, F. Hudson, A. Morello, and D. J. Reilly, *et al.*, Gate-based single-shot readout of spins in silicon, Nat. Nanotechnol. **14**, 437 (2019).

[18] F. Borjans, X. Mi, and J. Petta, Spin Digitizer for High-Fidelity Readout of a Cavity-Coupled Silicon Triple Quantum Dot, Phys. Rev. Appl. **15**, 044052 (2021).

[19] G. Zheng, N. Samkharadze, M. L. Noordam, N. Kalhor, D. Brousse, A. Sammak, G. Scappucci, and L. M. Vandersypen, Rapid gate-based spin read-out in silicon using an on-chip resonator, Nat. Nanotechnol. **14**, 742 (2019).

[20] P. Apostolidis, B. Villis, J. Chittock-Wood, A. Baumgartner, V. Vesterinen, S. Simbierowicz, J. Hassel, and M. Buitelaar, Quantum paraelectric varactors for radio-frequency measurements at mK temperatures, (2020), arXiv preprint ArXiv:2007.03588.

[21] S. Ilani, L. A. Donev, M. Kindermann, and P. L. McEuen, Measurement of the quantum capacitance of interacting electrons in carbon nanotubes, Nat. Phys. **2**, 687 (2006).

[22] M. Jarratt, S. Waddy, A. Jouan, A. Mahoney, G. Gardner, S. Fallahi, M. Manfra, and D. Reilly, Detection of the Quantum Capacitance of a Point Contact via Dispersive Gate Sensing, Phys. Rev. Appl. **14**, 064021 (2020).

[23] G. Badawy, S. Gazibegovic, F. Borsoi, S. Heedt, C.-A. Wang, S. Koelling, M. A. Verheijen, L. P. Kouwenhoven, and E. P. Bakkers, High mobility stemless InSb nanowires, Nano Lett. **19**, 3575 (2019).

[24] P. Krogstrup, N. Ziino, W. Chang, S. Albrecht, M. Madsen, E. Johnson, J. Nygård, C. M. Marcus, and T. Jespersen, Epitaxy of semiconductor–superconductor nanowires, Nat. Mater. **14**, 400 (2015).

[25] J. Hornibrook, J. Colless, A. Mahoney, X. Croot, S. Blanvillain, H. Lu, A. Gossard, and D. Reilly, Frequency multiplexing for readout of spin qubits, Appl. Phys. Lett. **104**, 103108 (2014).

[26] Good galvanic connection in this context means that the contact resistance R must be such that $2\pi/RC_G \gg f_0$. For $f_0 = 500$ MHz and $C_G = 1$ fF, this implies that $R \ll 10$ MΩ.

[27] D. Razmadze, D. Sabonis, F. K. Malinowski, G. C. Ménard, S. Pauka, H. Nguyen, D. M. van Zanten, C. Eoin, J. Suter, and P. Krogstrup, *et al.*, Radio-Frequency Methods for Majorana-Based Quantum Devices: Fast Charge Sensing and Phase-Diagram Mapping, Phys. Rev. Appl. **11**, 064011 (2019).

[28] D. de Jong, C. Prosko, D. Waardenburg, L. Han, F. K. Malinowski, P. Krogstrup, L. P. Kouwenhoven, J. V. Koski, and W. Pfaff, Rapid Microwave-Only Characterization and Readout of Quantum Dots Using Multiplexed Gigahertz-Frequency Resonators, Phys. Rev. Appl. **16**, 014007 (2021).

[29] T. Ihn, *Semiconductor Nanostructures: Quantum States and Electronic Transport* (Oxford university press, Oxford, 2010).

[30] We note that sensitivity is the most practical measure of measurement performance when the noise spectrum is white, which is explicitly violated here. In case the noise is white, the definition presented here would be equivalent to sensitivity measured using a sideband modulation. For the noise power monotonically decreasing with frequency, the sensitivity is a measure of the best-case performance if the integration time is longer, and worst-case performance if the integration time is shorter.

[31] D. Zajac, T. Hazard, X. Mi, E. Nielsen, and J. R. Petta, Scalable Gate Architecture for a One-Dimensional Array of Semiconductor Spin Qubits, Phys. Rev. Appl. **6**, 054013 (2016).

[32] M. Veldhorst, H. Eenink, C.-H. Yang, and A. S. Dzurak, Silicon CMOS architecture for a spin-based quantum computer, Nat. Commun. **8**, 1766 (2017).

[33] E. Chanrion, D. J. Niegemann, B. Bertrand, C. Spence, B. Jadot, J. Li, P.-A. Mortemousque, L. Hutin, R. Maurand, and X. Jehl, *et al.*, Charge Detection in an Array of CMOS Quantum Dots, Phys. Rev. Appl. **14**, 024066 (2020).

[34] Ö. Gül, D. J. Van Woerkom, I. van Weperen, D. Car, S. R. Plissard, E. P. Bakkers, and L. P. Kouwenhoven, Towards high mobility InSb nanowire devices, Nanotechnology **26**, 215202 (2015).

[35] S. L. Tomarken, Y. Cao, A. Demir, K. Watanabe, T. Taniguchi, P. Jarillo-Herrero, and R. Ashoori, Electronic Compressibility of Magic-Angle Graphene Superlattices, Phys. Rev. Lett. **123**, 046601 (2019).

[36] J. Eisenstein, L. Pfeiffer, and K. West, Negative Compressibility of Interacting Two-Dimensional Electron and Quasiparticle Gases, Phys. Rev. Lett. **68**, 674 (1992).

[37] L. Smith, A. Hamilton, K. Thomas, M. Pepper, I. Farrer, J. Griffiths, G. Jones, and D. Ritchie, Compressibility Measurements of Quasi-One-Dimensional Quantum Wires, Phys. Rev. Lett. **107**, 126801 (2011).

[38] A. Young, C. Dean, I. Meric, S. Sorgenfrei, H. Ren, K. Watanabe, T. Taniguchi, J. Hone, K. Shepard, and P. Kim, Electronic compressibility of layer-polarized bilayer graphene, Phys. Rev. B **85**, 235458 (2012).

[39] J. Martin, B. E. Feldman, R. T. Weitz, M. T. Allen, and A. Yacoby, Local Compressibility Measurements of Correlated States in Suspended Bilayer Graphene, Phys. Rev. Lett. **105**, 256806 (2010).

[40] V. Venkatachalam, A. Yacoby, L. Pfeiffer, and K. West, Local charge of the $\nu = 5/2$ fractional quantum Hall state, Nature **469**, 185 (2011).

[41] X. Wen and A. Zee, Compressibility and superfluidity in the fractional-statistics liquid, Phys. Rev. B **41**, 240 (1990).

[42] D. Nozadze and N. Trivedi, Compressibility as a probe of quantum phase transitions in topological superconductors, Phys. Rev. B **93**, 064512 (2016).

[43] C. Barthel, M. Kjærgaard, J. Medford, M. Stopa, C. M. Marcus, M. Hanson, and A. C. Gossard, Fast sensing of

double-dot charge arrangement and spin state with a radio-frequency sensor quantum dot, Phys. Rev. B **81**, 161308 (2010).

[44] M. Urdampilleta, D. J. Niegemann, E. Chanrion, B. Jadot, C. Spence, P.-A. Mortemousque, C. Bäuerle, L. Hutin, B. Bertrand, and S. Barraud, *et al.*, Gate-based high fidelity spin readout in a CMOS device, Nat. Nanotechnol. **14**, 737 (2019).

[45] D. Keith, M. House, M. Donnelly, T. Watson, B. Weber, and M. Simmons, Single-shot spin readout in semiconductors near the shot-noise sensitivity limit, Phys. Rev. X **9**, 041003 (2019).

[46] Y.-P. Shim, R. Ruskov, H. M. Hurst, and C. Tahan, Induced quantum dot probe for material characterization, Appl. Phys. Lett. **114**, 152105 (2019).

[47] https://doi.org/10.5281/zenodo.6880890.

[48] D. M. Pozar, *Microwave Engineering* (John wiley & sons, 2011).

[49] M. Khalil, M. Stoutimore, F. Wellstood, and K. Osborn, An analysis method for asymmetric resonator transmission applied to superconducting devices, J. Appl. Phys. **111**, 054510 (2012).

[50] J. Van Veen, D. De Jong, L. Han, C. Prosko, P. Krogstrup, J. D. Watson, L. P. Kouwenhoven, and W. Pfaff, Revealing charge-tunneling processes between a quantum dot and a superconducting island through gate sensing, Phys. Rev. B **100**, 174508 (2019).

[51] https://www.minicircuits.com/WebStore/dashboard.html?model=ZEDC-15-2B.

[52] https://www.cosmicmicrowavetechnology.com/citlf2.